Acceleron Aerospace Journal || AAJ.11.2106-2429
Volume 2, Issue 6, pp (346-367)
Research Paper
E-ISSN- 2583-9942 || DOI: 10.61359/11.2106-2429

Analytical Solution to the Steady Navier-Stokes Equation for a Supersonic Cone in the Area of Boundary Layer Behind the Shock Wave by Means Tunnel Mathematics

Oleh G. Shvydkyi*

ORCID: 0000-0002-8038-8775

Independent researcher, Zaporizhzhia, Ukraine

Abstract: The means of tunnel mathematics (the theory of functions of a spatial complex variable) allow for an analytical solution to the problem of supersonic flow around a cone in the area of the boundary layer and beyond. The peculiar feature of the Navier-Stokes equations is that they allow for the determination of analytical velocity fields of fluids only for a small number of simple problems. Of course, the problem of the supersonic motion of fluid around a cone is not included in this number. Tunnel mathematics is a method for finding analytical vector velocity fields for steady flows of fluids with axial symmetry. The Navier-Stokes equations are then used to determine pressure and temperature distributions. The main theorem of tunnel mathematics allows for the determination of these distributions for planes z = const (similar to constructing slices of a brain in an MRI procedure). By collecting these "slices," we can obtain full space distributions of pressure and temperature around a supersonic cone. At this stage of investigation, the conclusions obtained through tunnel mathematics make it possible to qualitatively assess the thickness of the boundary layer on the cone's surface, the shape of the shock wave, and whether the shock wave intersects the boundary layer. First of all, we focused on ensuring that the resulting solutions corresponded to the physical pattern of phenomena. No doubt, solutions obtained through tunnel mathematics must be confirmed experimentally.

Table of Contents

1. Introduction

It is well known from the classical works **[6]** and **[1]** that an analytical solution to the problem of flow past a cone is possible only in the limit of small vertex angles of the cone. In this case, the solution pertains only to the potential flow outside the boundary layer area. Tunnel mathematics is not subject to such restrictions. The case of arbitrary vertex angles of a cone usually requires the application of numerical methods **[3, 4],** and time-consuming graphical methods are also used **[5, 7].** Such solutions do not pertain to the boundary layer area, but only to the potential flow outside it. The current state of affairs in the theory of heating and transition in a hypersonic boundary layer can be found in works **[9]** and **[10].** From the perspective of energy conservation, aerodynamic heating in a hypersonic boundary layer is considered in **[11]** and **[12].** The boundary layer is an intriguing hybrid that arises from the interaction of two potential fields: the electrostatic attraction field from the cone wall and the vector velocity field of the main fluid stream. Therefore, it is plausible that a boundary layer can be described using tunnel mathematics, as the theory of complex variables tends to describe potential fields. Furthermore, tunnel mathematics enables the use of ordinary mathematical analysis, which has long been supplanted in fluid dynamics by numerical methods. Examples of the application of tunnel mathematics to describe the boundary layer in compressible and incompressible fluid flows over a rotating disk can be found in **[15]** and **[16]**.

*Research Scholar, Independent researcher, Zaporizhzhia, Ukraine. **Corresponding Author: oleg.shv.jw@gmail.com.**
** Received: 14-July-2024 || Revised: 28-July-2024 || Accepted: 30-July-2024 || Published Online: 30-July-2024.

2. Theoretical Overview

The flow past a cone is schematically shown in Figure 1. We work in modified spherical system of coordinates; i.e. we measure angle θ from xy-plane (not from z axis, as usually). So, we need carry out following transformation with ordinary spherical system of coordinates:

$$v_\theta \to -v_\theta;$$
$$\theta \to \frac{\pi}{2} - \theta; \quad (1)$$
$$\partial\theta \to -\partial\theta.$$

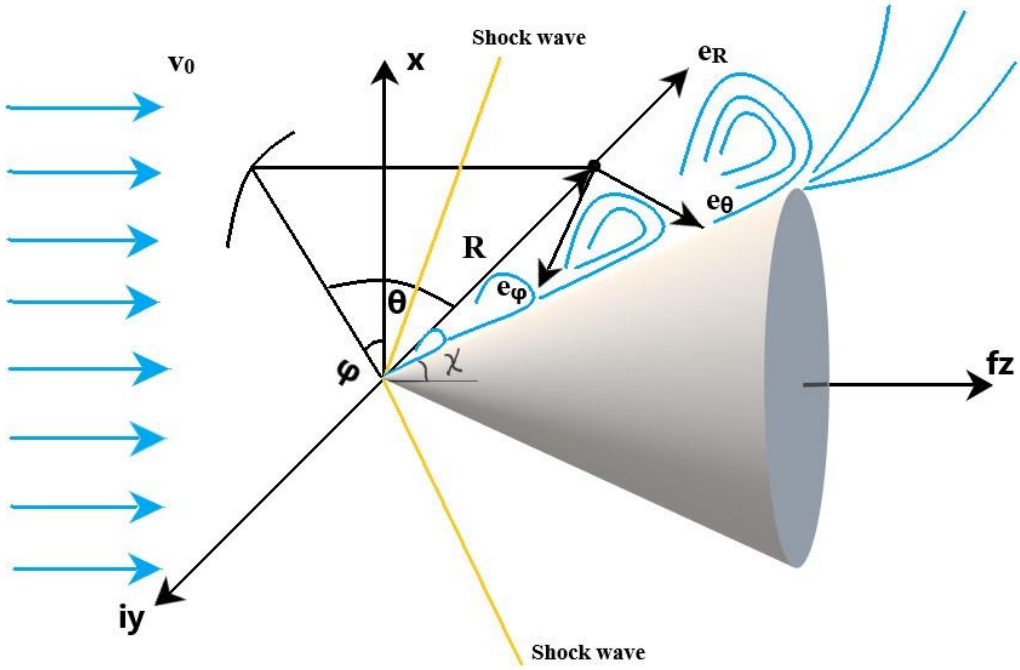

Figure 1. The supersonic flow past a cone (χ is a half of vertical angle of cone, e_R, e_θ, e_φ are the unity orts of spherical system of coordinates, v_0 is the vector of incident flow velocity; we measure angle θ from xy plane (not from z axis, as usually)).

Tunnel mathematics equations applied to the components of the vector velocity field in Cartesian coordinate system look like this [14]:

$$\frac{\partial u}{\partial x} + \frac{(uw)y}{(x^2+y^2)^{3/2}}\left(2+\left(\frac{y}{x}\right)^2\right) + \frac{1}{\sqrt{x^2+y^2}}\frac{\partial(vw)}{\partial x} = \frac{\partial v}{\partial y} - \frac{(vw)x}{(x^2+y^2)^{3/2}}\left(2+\left(\frac{x}{y}\right)^2\right) - \frac{1}{\sqrt{x^2+y^2}}\frac{\partial(uw)}{\partial y}$$
$$= -\frac{2y}{\sqrt{x^2+y^2}}\frac{\partial u}{\partial z} + \frac{1}{x}\cdot\frac{\partial(uw)}{\partial z} + \frac{1}{y}\cdot\frac{\partial(vw)}{\partial z} - \frac{2y}{(x^2+y^2)}\frac{\partial(vw)}{\partial z}; \quad (2)$$

$$\frac{\partial v}{\partial x} + \frac{(vw)y}{(x^2+y^2)^{3/2}} - \frac{1}{\sqrt{x^2+y^2}}\frac{\partial(uw)}{\partial x} = -\frac{\partial u}{\partial y} + \frac{(uw)x}{(x^2+y^2)^{3/2}} - \frac{1}{\sqrt{x^2+y^2}}\frac{\partial(vw)}{\partial y}$$
$$= -\frac{2y}{\sqrt{x^2+y^2}}\frac{\partial v}{\partial z} + \frac{2y}{(x^2+y^2)}\frac{\partial(uw)}{\partial z}; \quad (3)$$

$$\frac{1}{x}\cdot\frac{\partial(uw)}{\partial x} + \frac{1}{y}\cdot\frac{\partial(vw)}{\partial x} = -\frac{i}{y}\cdot\frac{\partial(vw)}{\partial y} - \frac{i}{x}\cdot\frac{\partial(uw)}{\partial y}$$
$$= -\frac{\partial u}{\partial z} - i\frac{\partial v}{\partial z} + \frac{i}{\sqrt{x^2+y^2}}\cdot\frac{\partial(uw)}{\partial z} - \frac{1}{\sqrt{x^2+y^2}}\cdot\frac{\partial(vw)}{\partial z}. \quad (4)$$

It is easy seen that at $w = 0$ these equations transform into ordinary plane Cauchy-Riemann conditions (12) and (13).

$$\Delta u = 0; \quad (5)$$
$$\Delta v = 0; \quad (6)$$
$$(uw)y^3 = (vw)x^3; \quad (7)$$
$$\Delta(uw) = \frac{(vw)x}{y^3} - \frac{(y^2-x^2)}{xy}C_i - C_r; \quad (8)$$

$$\Delta(vw) = \frac{(uw)y}{x^3} - \frac{(y^2-x^2)}{xy}C_r + C_i; \quad \textbf{(9)}$$

where constants C_r and C_i are included in the following relations:

$$\frac{\partial(uw)}{\partial x} + i\frac{\partial(uw)}{\partial y} = (C_r + iC_i)x; \quad \textbf{(10)}$$

$$\frac{\partial(vw)}{\partial x} + i\frac{\partial(vw)}{\partial y} = -(C_r + iC_i)y. \quad \textbf{(11)}$$

Relations (10) and (11) result from (4).

In (5), (6), (8), (9) $\Delta = \frac{\partial^2}{\partial x^2} + \frac{\partial^2}{\partial y^2}$ is the Laplace operator on the *xy* plane.

Also, the ordinary Cauchy-Riemann conditions hold on the *xy* plane [8]:

$$\frac{\partial u}{\partial x} = \frac{\partial v}{\partial y}; \quad \textbf{(12)}$$

$$\frac{\partial v}{\partial x} = -\frac{\partial u}{\partial y}. \quad \textbf{(13)}$$

Functions *u*, *v*, *w* in (2) – (13) correspond to the vector velocity field components in Cartesian coordinate system. So, such relations connect vector velocity field components in Cartesian and modified (1) spherical coordinate systems:

$$u = v_x = \cos\varphi\,(v_R\cos\theta - v_\theta\sin\theta) - v_\varphi\sin\varphi\,; \quad \textbf{(14)}$$

$$v = v_y = \sin\varphi\,(v_R\cos\theta - v_\theta\sin\theta) + v_\varphi\cos\varphi\,; \quad \textbf{(15)}$$

$$w = v_z = v_R\sin\theta + v_\theta\cos\theta\,; \quad \textbf{(16)}$$

There are also inverse transition formulas:

$$v_R = \cos\theta\,(u\cos\varphi + v\sin\varphi) + w\sin\theta\,; \quad \textbf{(17)}$$

$$v_\theta = -\sin\theta\,(u\cos\varphi + v\sin\varphi) + w\cos\theta\,; \quad \textbf{(18)}$$

$$v_\varphi = -u\sin\varphi + v\cos\varphi\,; \quad \textbf{(19)}$$

and ordinary transition formulas between Cartesian and modified (1) spherical coordinate systems hold:

$$x = R\cos\theta\cos\varphi\,; \quad \textbf{(20)}$$

$$y = R\cos\theta\sin\varphi\,; \quad \textbf{(21)}$$

$$z = R\sin\theta. \quad \textbf{(22)}$$

Recall that we work in modified spherical system of coordinates; i. e. *we measure angle θ from xy plane (not from z axis as usually)* (Fig. 1).

Taking into account that problem of flow past a cone has axial symmetry, i.e. $v_\varphi = 0$, we can obtain from (14) – (16) following relations:

$$(uw) = \cos\varphi\left((v_R^2 - v_\theta^2)\frac{\sin 2\theta}{2} + v_R v_\theta\cos 2\theta\right); \quad \textbf{(23)}$$

$$(vw) = \sin\varphi\left((v_R^2 - v_\theta^2)\frac{\sin 2\theta}{2} + v_R v_\theta\cos 2\theta\right); \quad \textbf{(24)}$$

Therefore, taking into account (20) and (21) we can conclude that for our problem with axial symmetry we have following exact relation:

$$(uw)y = (vw)x. \quad \textbf{(25)}$$

We see that (25) differs from (7).

Also, using well known formula

$$\Delta(uw) = u\Delta w + w\Delta u + 2\nabla u\nabla w, \quad \textbf{(26)}$$

and taking into account (5) and assumption that $\Delta w = 0$, we obtain the relation which work on *xy* plane:

$$\Delta(uw) = 2\nabla u\nabla w = 2\left(\frac{\partial u}{\partial R}\frac{\partial w}{\partial R} + \frac{\partial u}{R\partial\theta}\frac{\partial w}{R\partial\theta}\right). \quad \textbf{(27)}$$

Using (14), (16), (8) and (24) we arrive to the following approximate formulas:

$$\left(\frac{\partial v_R}{\partial R}\right)^2 - \left(\frac{\partial v_\theta}{\partial R}\right)^2 + \frac{1}{R^2}\left(\left(\frac{\partial v_R}{\partial\theta} - v_\theta\right)^2 - \left(\frac{\partial v_\theta}{\partial\theta} + v_R\right)^2\right) \sim v_R^2 - v_\theta^2; \quad \textbf{(28)}$$

$$\frac{\partial v_R}{\partial R}\cdot\frac{\partial v_\theta}{\partial R} + \frac{1}{R^2}\left(\frac{\partial v_R}{\partial\theta} - v_\theta\right)\left(\frac{\partial v_\theta}{\partial\theta} + v_R\right) \sim v_R v_\theta\,. \quad \textbf{(29)}$$

Recall that (28) and (29) work on *xy* plane ($z = const$) only!

3. Results and Discussions

4.1 Construction of vector velocity fields

Using (2) – (4), (12), (13) and (25) we can find the expressions for functions *(uw)* and *(vw)*:

$$(uw) = \frac{A_0^2 r_0^2 a}{y(x^2+y^2)} \exp\left[z\sqrt{x^2+y^2}\left(\frac{4xy}{(x^2+y^2)^2}+\frac{1}{xy}\right)\right]; \quad (30)$$

$$(vw) = \frac{A_0^2 r_0^2 a}{x(x^2+y^2)} \exp\left[z\sqrt{x^2+y^2}\left(\frac{4xy}{(x^2+y^2)^2}+\frac{1}{xy}\right)\right]; \quad (31)$$

where A_0, r_0, a are the constants; $[A_0] = \frac{m}{sec}$; $[r_0] = [a] = m$.

Now we can construct the components of vector velocity field in Cartesian coordinate system. In order to satisfy (25) we select the components of analytical function [8] in following manner:

$$u = A_0 \frac{x}{a}; \quad (32)$$

$$v = A_0 \frac{y}{a}. \quad (33)$$

It is easy seen that (5) and (6) are satisfied automatically.

$$w = A_0 \frac{(r_0 a)^2}{xy(x^2+y^2)} \exp\left[z\sqrt{x^2+y^2}\left(\frac{4xy}{(x^2+y^2)^2}+\frac{1}{xy}\right)\right]; \quad (34)$$

Now using (17), (18), (20) – (22) we can obtain the components of vector velocity field in modified (1) spherical coordinate system:

$$v_R = A_0\left(\frac{(R\cos\theta)}{a}\cos\theta + \sin\theta \frac{2(r_0 a)^2}{A_2(R\cos\theta)^4}\exp[2A_1\, tan\,\theta]\right); \quad (35)$$

$$v_\theta = A_0\left(-\frac{(R\cos\theta)}{a}\sin\theta + \cos\theta \frac{2(r_0 a)^2}{A_2(R\cos\theta)^4}\exp[2A_1\, tan\,\theta]\right); \quad (36)$$

where $A_1\ and\ A_2$ are dimensionless constants (they depend on φ).

It is well known that a shock wave on a supersonic cone is formed as a result of interaction of incident and reflected flows of fluid. *So, it is naturally to find a shape of a shock wave as a result of intersection of mathematical surfaces describing the vector velocity fields of incident and reflected flows.* In order to do this, we need to impose the boundary conditions on (35) and (36).

In front of the shock wave (Figure 1) the velocity of incident flow (without taking into account the interaction with reflected flow) has such simple form:

$$v_R = v_0 \sin\theta \text{ and } v_\theta = v_0 \cos\theta; \quad (37)$$

where v_0 is a magnitude of velocity of incident flow:

$$v = \sqrt{v_R^2 + v_\theta^2} = v_0. \quad (38)$$

Behind the shock wave such boundary condition holds:

$$\text{at } \theta = \theta_w = \frac{\pi}{2} - \chi \text{ should be } v_R = 0 \text{ and } v_\theta = 0; \quad (39)$$

where χ is a half of vertical angle of cone (Figure 1); this is so called non-slip boundary condition.

In order to satisfy (39) the relations (35) and (36) must take such form:

$$v_R = A_0\left(\frac{(R\cos\theta)}{a}\cos\theta + + \sin\theta \frac{2(r_0 a)^2}{A_2(R\cos\theta)^4}\left[\frac{A_2(R\cos\theta_w)^5}{2(r_0 a)^2 a}\frac{1}{tan\,\theta_w}\right]^{\frac{tan\,\theta}{tan\,\theta_w}}\cos\pi\frac{tan\,\theta}{tan\,\theta_w}\right); \quad (40)$$

$$v_\theta = A_0\left(-\frac{(R\cos\theta)}{a}\sin\theta + \cos\theta \frac{2(r_0 a)^2}{A_2(R\cos\theta)^4}\left[\frac{A_2(R\cos\theta_w)^5}{2(r_0 a)^2 a}tan\,\theta_w\right]^{\frac{tan\,\theta}{tan\,\theta_w}}\right); \quad (41)$$

The magnitude of velocity behind the shock wave take such form:

$$v = \sqrt{v_R^2 + v_\theta^2} = A_0\left(\left(\frac{R\cos\theta}{a}\right)^2 + \sin 2\theta \frac{2(r_0 a)^2}{aA_2(R\cos\theta)^3}\left[\frac{A_2(R\cos\theta_w)^5}{2(r_0 a)^2 a}\right]^{\frac{tan\,\theta}{tan\,\theta_w}} \times \left([tan\,\theta_w]^{-\frac{tan\,\theta}{tan\,\theta_w}}\cdot\cos\pi\frac{tan\,\theta}{tan\,\theta_w} - [tan\,\theta_w]^{\frac{tan\,\theta}{tan\,\theta_w}}\right) + \left(\frac{2(r_0 a)^2}{A_2(R\cos\theta)^4}\right)^2 \times \left[\frac{A_2(R\cos\theta_w)^5}{2(r_0 a)^2 a}\right]^{\frac{2\,tan\,\theta}{tan\,\theta_w}} \times \left([tan\,\theta_w]^{-\frac{2tan\,\theta}{tan\,\theta_w}}\cdot\sin^2\theta + [tan\,\theta_w]^{\frac{2\,tan\,\theta}{tan\,\theta_w}}\cdot\cos^2\theta\right)\right)^{\frac{1}{2}}. \quad (42)$$

Below in Figure. 2 – 4 the surfaces of discontinuity for component v_R formed by (37) and (40) are shown at $\chi = 10°$ ($\theta_w = 80°$ (1.4 rad)) and different velocities of incident flow.

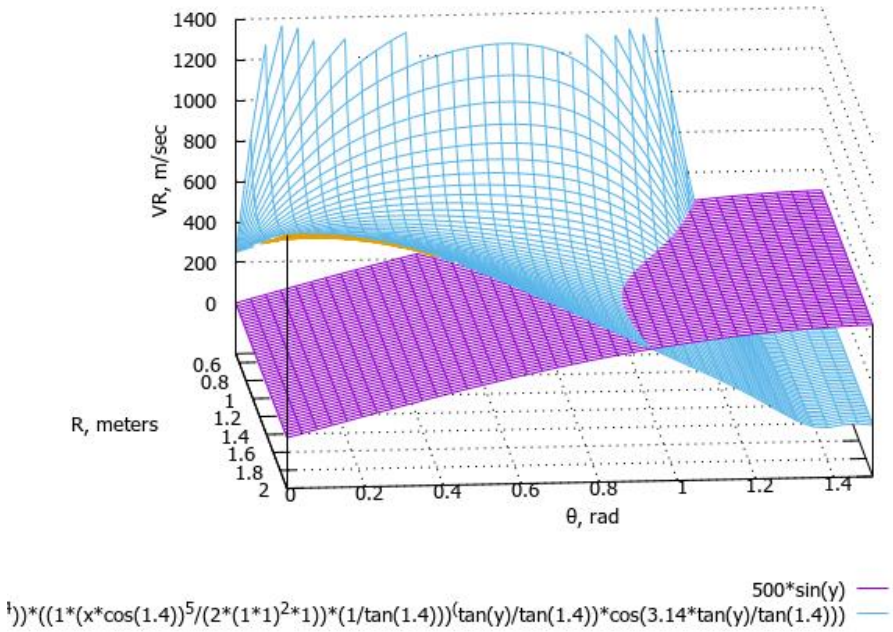

Figure 2. Surface of discontinuity for component v_R formed by (37) and (40) at $\chi = 10°$ ($\theta_w = 80°$ ($1.4\ rad$)) and $v_0 = 500\ \frac{m}{sec}$ (supersonic case).

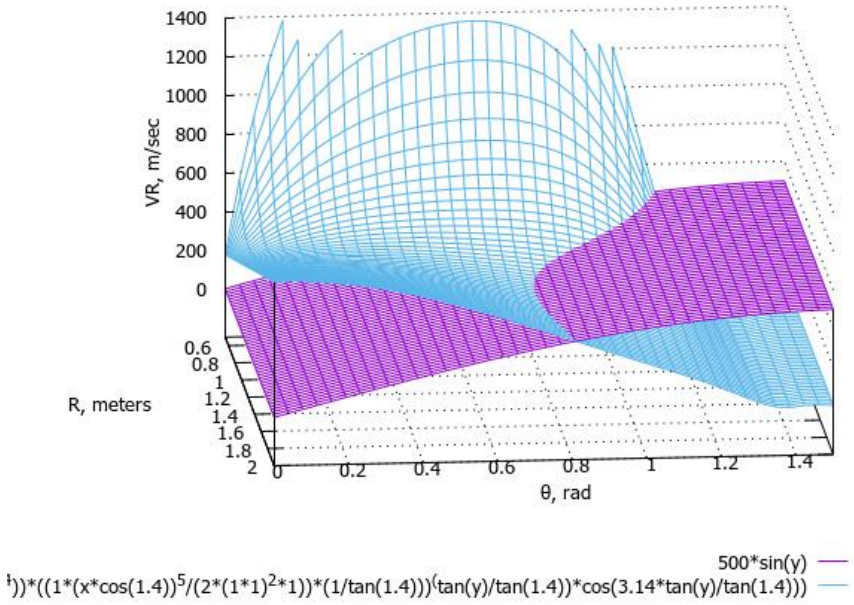

Figure 3. Surface of discontinuity for component v_R formed by (37) and (40) at $\chi = 10°$ ($\theta_w = 80°$ ($1.4\ rad$)) and $v_0 = 350\ \frac{m}{sec}$ (transonic case).

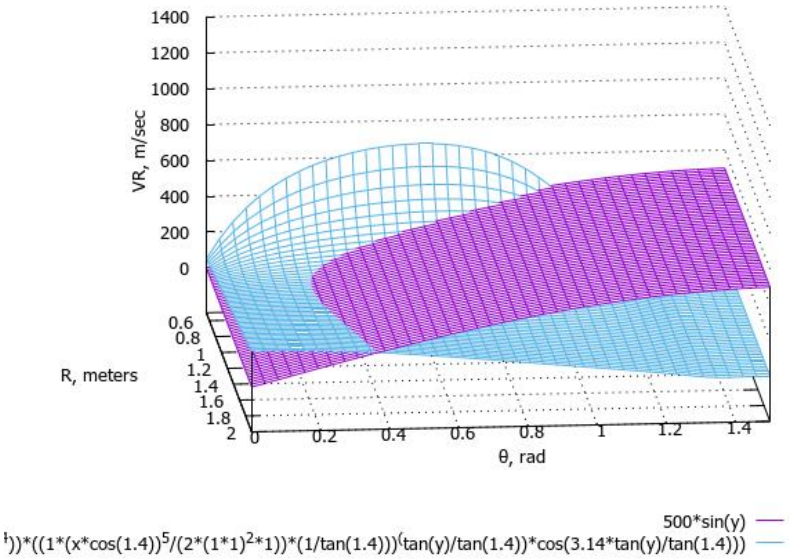

Figure 4. Surface of discontinuity for component v_R formed by (37) and (40) at $\chi = 10°$ ($\theta_w = 80°$ ($1.4\ rad$)) and $v_0 = 100\ \frac{m}{sec}$ (subsonic case).

It is easy seen from Figs. 2 – 4 that the lower the velocity of incident flow v_0, the smaller the values of the angles θ the shock wave acquires (*we measure angle θ from xy plane (not from z axis as usually)* (Figure 1)). This behavior of the shock wave fully corresponds to the physical pattern of phenomena.

Below in Figs. 5 – 7 the surfaces of discontinuity for component v_R formed by (37) and (40) are shown at $\chi = 20°$ ($\theta_w = 70°$ ($1.2\ rad$)) and different velocities of incident flow.

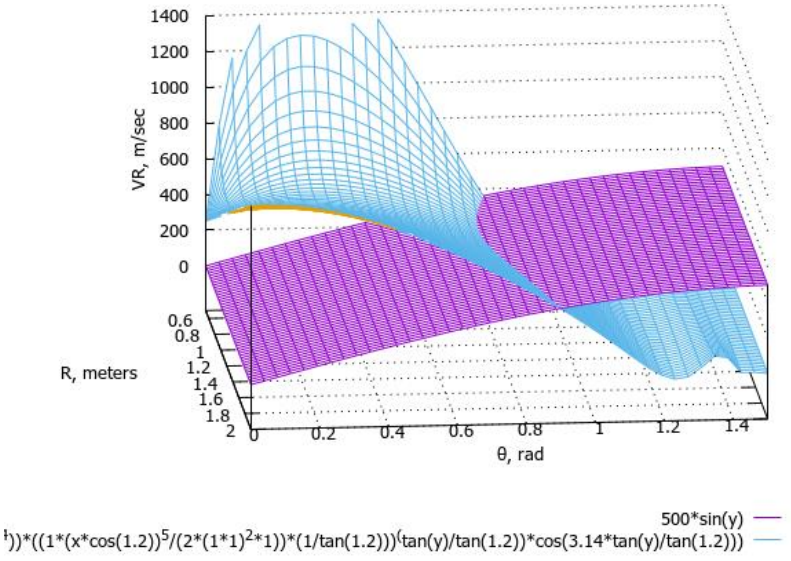

Figure 5. Surface of discontinuity for component v_R formed by (37) and (40) at $\chi = 20°$ ($\theta_w = 70°$ ($1.2\ rad$)) and $v_0 = 500\ \frac{m}{sec}$ (supersonic case).

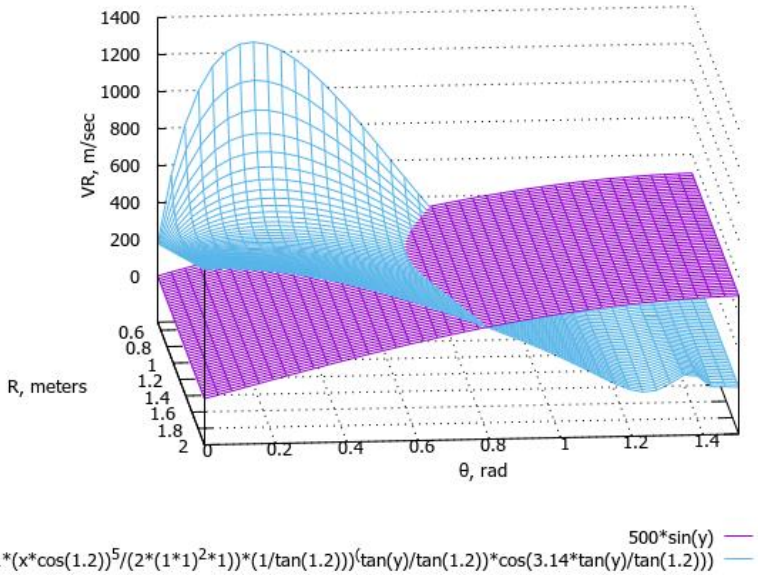

Figure 6. Surface of discontinuity for component v_R formed by (37) and (40) at $\chi = 20°$ ($\theta_w = 70°$ ($1.2\ rad$)) and $v_0 = 350\ \frac{m}{sec}$ (transonic case).

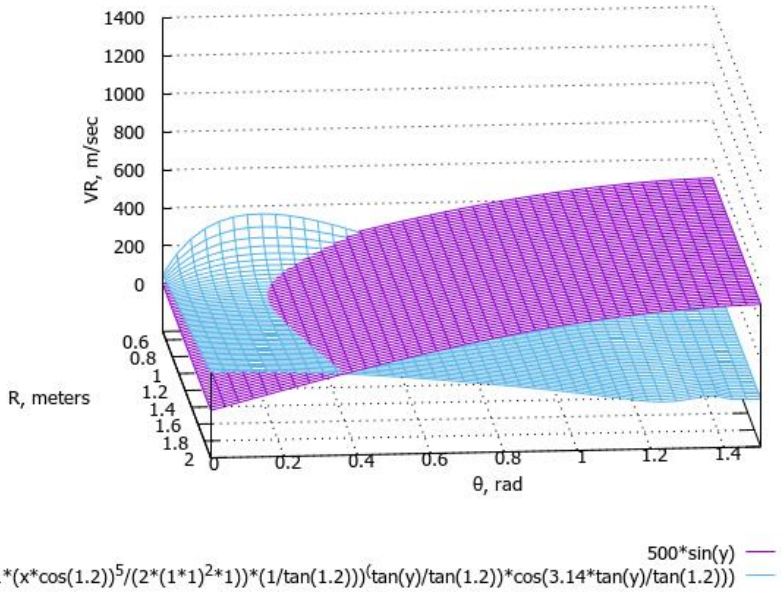

Figure 7. Surface of discontinuity for component v_R formed by (37) and (40) at $\chi = 20°$ ($\theta_w = 70°$ ($1.2\ rad$)) and $v_0 = 100\ \frac{m}{sec}$ (subsonic case).

Comparing Figs. 5 – 7 with Figs. 2 – 4 we see that the larger the vertical angle of cone, the smaller the values of the angles θ the shock wave acquires. This behavior of the shock wave fully corresponds to the physical pattern of phenomena as well.

Below in Figs. 8 – 10 the surfaces of discontinuity for component v_θ formed by (37) and (41) are shown at $\chi = 10°$ ($\theta_w = 80°$ $(1.4\,rad)$) and different velocities of incident flow.

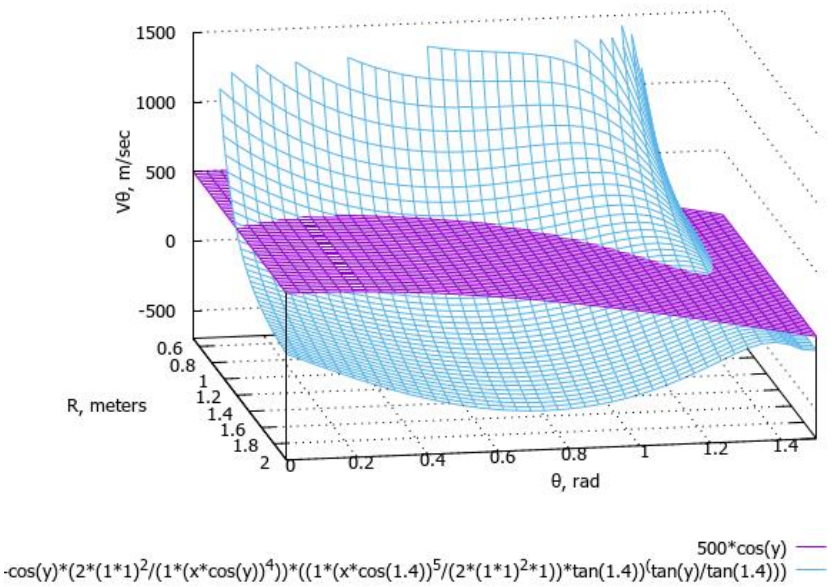

Figure 8. Surface of discontinuity for component v_θ formed by (37) and (41) at $\chi = 10°$ ($\theta_w = 80°$ $(1.4\,rad)$) and $v_0 = 500\ \frac{m}{sec}$ (supersonic case).

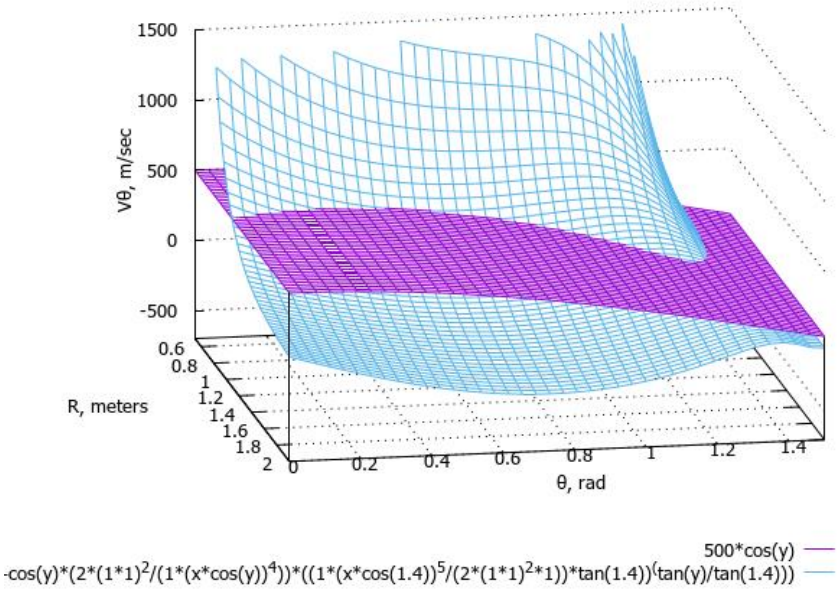

Figure 9. Surface of discontinuity for component v_θ formed by (37) and (41) at $\chi = 10°$ ($\theta_w = 80°$ $(1.4\,rad)$) and $v_0 = 350\ \frac{m}{sec}$ (transonic case).

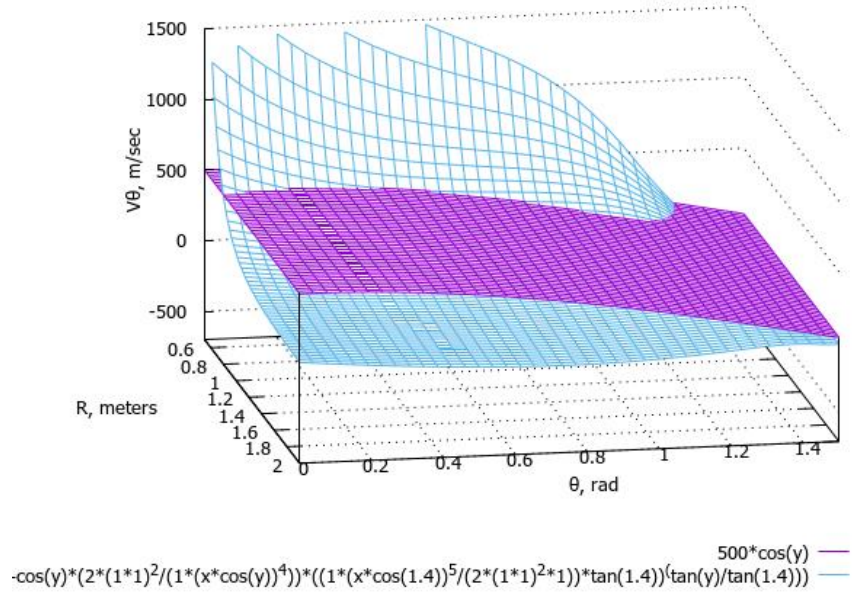

Figure 10. Surface of discontinuity for component v_θ formed by (37) and (41) at $\chi = 10°$ ($\theta_w = 80°$ ($1.4\ rad$)) and $v_0 = 100\ \frac{m}{sec}$ (subsonic case).

Below in Figs. 11 – 13 the surfaces of discontinuity for component v_θ formed by (37) and (41) are shown at $\chi = 20°$ ($\theta_w = 70°$ ($1.2\ rad$)) and different velocities of incident flow.

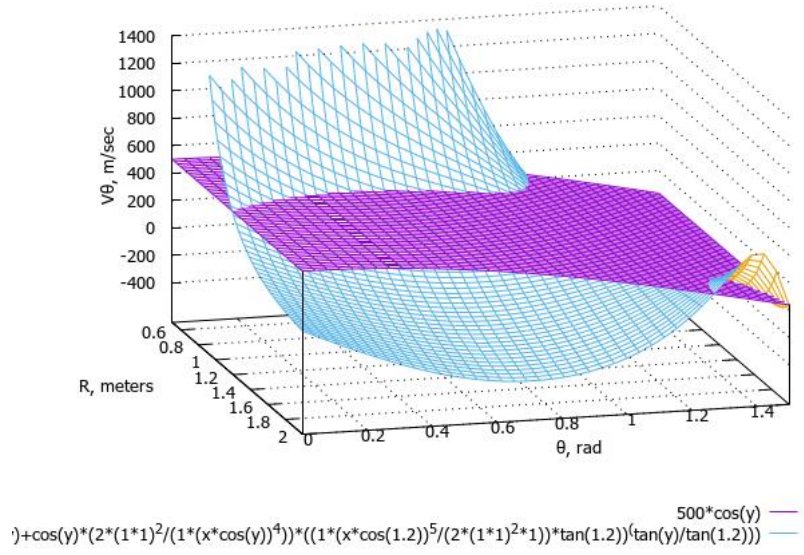

Figure 11. Surface of discontinuity for component v_θ formed by (37) and (41) at $\chi = 20°$ ($\theta_w = 70°$ ($1.2\ rad$)) and $v_0 = 500\ \frac{m}{sec}$ (supersonic case).

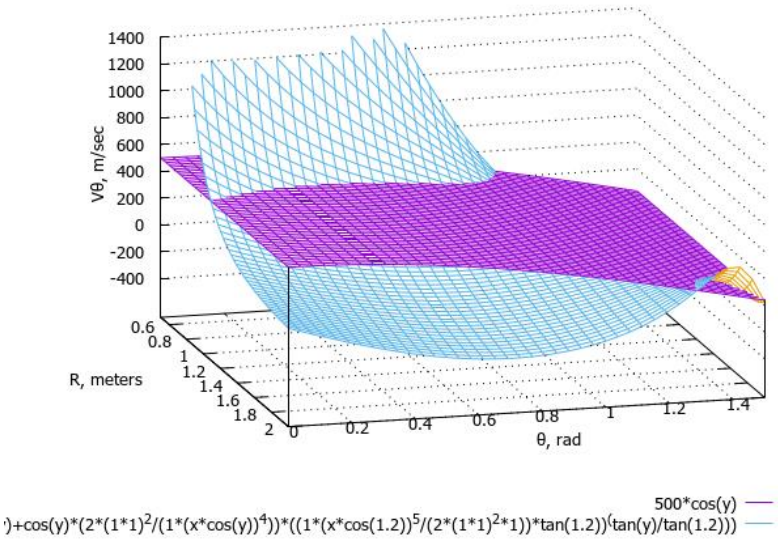

Figure 12. Surface of discontinuity for component v_θ formed by (37) and (41) at $\chi = 20°$ ($\theta_w = 70°$ ($1.2\ rad$)) and $v_0 = 350\ \frac{m}{sec}$ (transonic case).

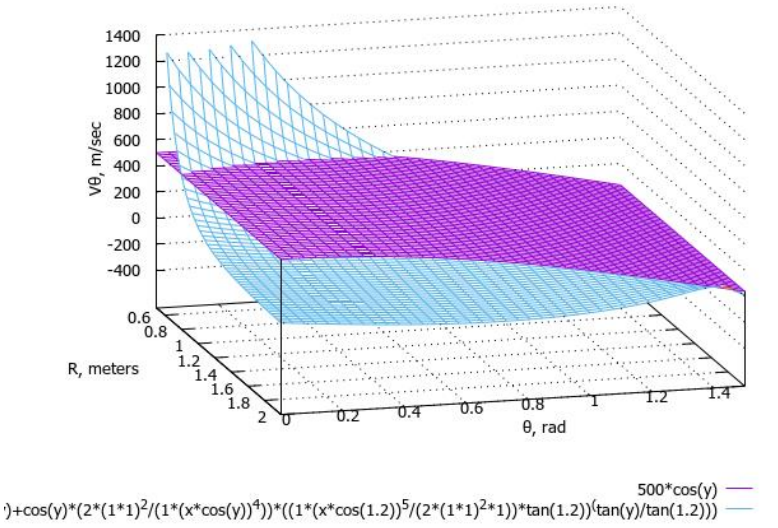

Figure 13. Surface of discontinuity for component v_θ formed by (37) and (41) at $\chi = 20°$ ($\theta_w = 70°$ ($1.2\ rad$)) and $v_0 = 100\ \frac{m}{sec}$ (subsonic case).

Behavior of the surfaces of discontinuity for component v_θ is fully similar to that for component v_R. Also, it is seen that formulas (40) and (41) allow to correctly determine the values of angles θ for the shock wave only at approximately $R \leq 1.2$ meter. Some discrepancies of angles θ for the surfaces of discontinuity for corresponding components v_θ and v_R may indicate that the shock wave has a certain thickness (such uneven thickness of the shock wave is a dominantly consequence of "smeared" spatial change of component v_R). Figs. 8 – 13 shows that surfaces of discontinuity for component v_θ are more like a right cone than ones for component v_R. This similarity becomes more and more evident at higher speeds and smaller vertical angles of cone.

Tending to infinity (especially for small R) of graphs corresponding to (40) and (41) in Figs. 2 – 13 results from the presence of R in denominator. However, this problem can be solved by way corresponding adjustment of calibration coefficients A_2, r_0, a to which at graph building the value 1 was assigned.
Where graphs corresponding to (40) and (41) in Figs. 2 – 13 reach maximums (especially it is well seen for small R) the boundary layer begins. So, we can conclude that *shock waves intersect boundary layers on all figures.*

Below in Figs. 14, 15 the surfaces of discontinuity for velocity magnitude v formed by (38) and (42) are shown at $\chi = 10°$ ($\theta_w = 80°$ ($1.4\ rad$)) and different velocities of incident flow.

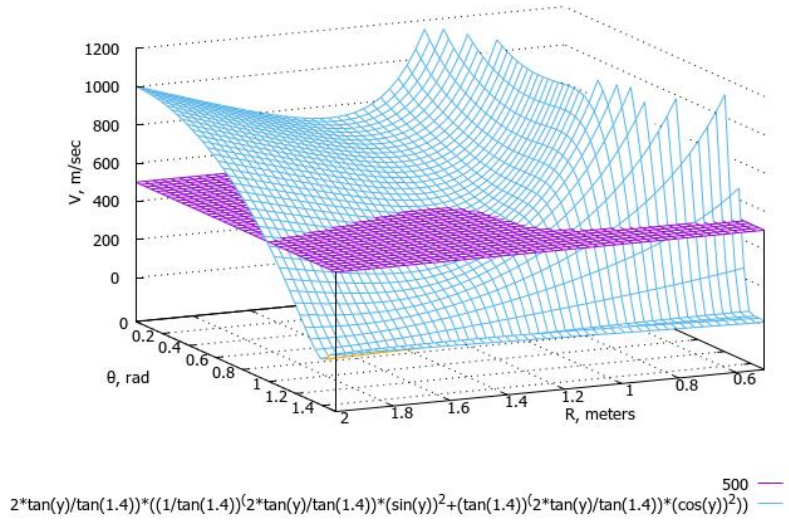

Figure 14. Surface of discontinuity for velocity magnitude v formed by (38) and (42) at $\chi = 10°$ ($\theta_w = 80°$ ($1.4\ rad$)) and $v_0 = 500\ \frac{m}{sec}$ (supersonic case).

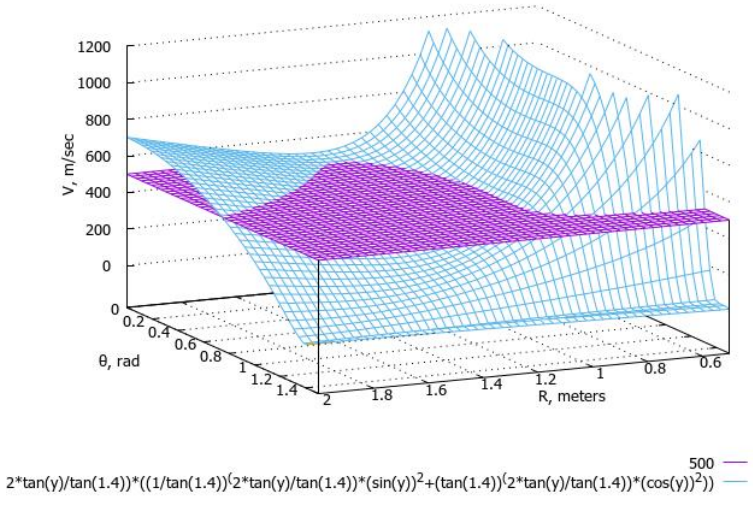

Figure 15. Surface of discontinuity for velocity magnitude v formed by (38) and (42) at $\chi = 10°$ ($\theta_w = 80°$ ($1.4\ rad$)) and $v_0 = 350\ \frac{m}{sec}$ (transonic case).

Below in Figs. 16, 17 the surfaces of discontinuity for velocity magnitude v formed by (38) and (42) are shown at $\chi = 20°$ ($\theta_w = 70°$ $(1.2\,rad)$) and different velocities of incident flow.

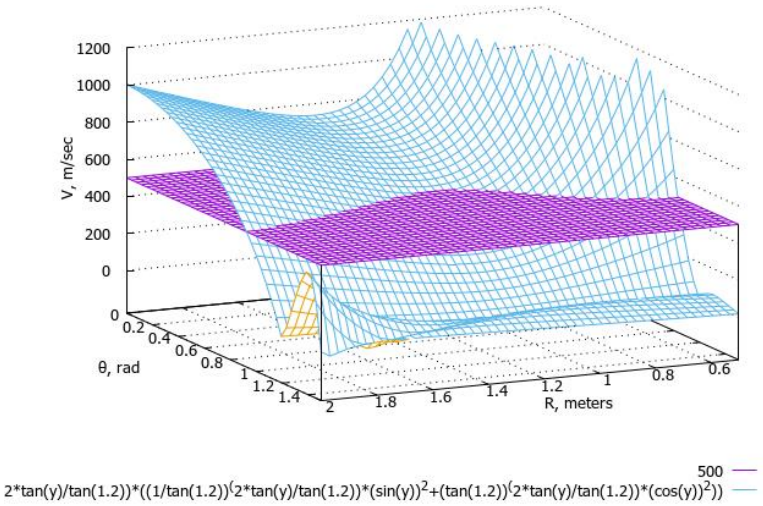

Figure 16. Surface of discontinuity for velocity magnitude v formed by (38) and (42) at $\chi = 20°$ ($\theta_w = 70°$ $(1.2\,rad)$) and $v_0 = 500\ \frac{m}{sec}$ (supersonic case).

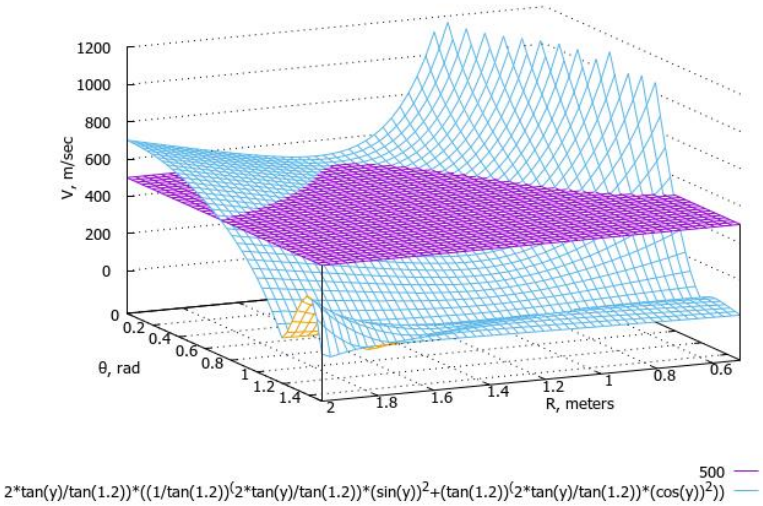

Figure 17. Surface of discontinuity for velocity magnitude v formed by (38) and (42) at $\chi = 20°$ ($\theta_w = 70°$ $(1.2\,rad)$) and $v_0 = 350\ \frac{m}{sec}$ (transonic case).

It is seen from Figs. 14 – 17 that the smaller the vertical angle of cone and the higher the velocity of incident flow, the better the shape of shock wave coincides with a right cone.
In general case, the shape of shock wave is a flared cone.

4.2 Calculation of the temperature distribution.

4.2.1 Preliminary calculations (equation of continuity, Navier-Stokes equations for a compressible flow).

Mathematical analysis of (30) and (31) in the light of relations (2) – (4) shows that relations (30) and (31) are fulfilled on the intersection of two surfaces:

$$z = -\frac{x^3(x^2+y^2)^{3/2}}{y((y^2-x^2)^2+8x^4)}; \quad \textbf{(43)}$$

$$z = -\frac{y^3(x^2+y^2)^{3/2}}{x((y^2-x^2)^2+8y^4)}. \quad \textbf{(44)}$$

The intersection of (43) and (44) is shown below on Figure 18.

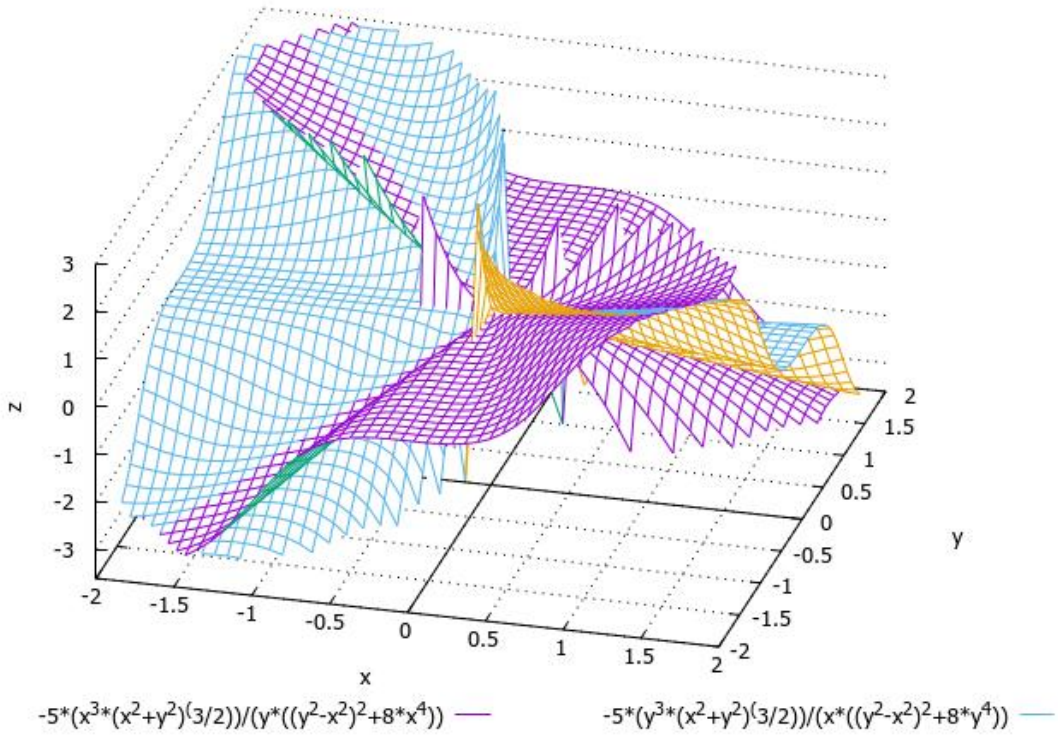

Figure 18. Intersection of surfaces (43) (blue) and (44) (cyan).

It is seen from Figure 18 that parts of the intersection of surfaces (43) and (44) at $y = \pm x$ resemble the shape of a shock wave on a supersonic cone. Taking into account (25), (20) (21) and axial symmetry of our problem, we can conclude that relations (30) and (31) and their derivatives are well suited to describe a supersonic flow past a cone.

Using (34) and (2) – (4) we can find Laplacian of *w* on the *xy* plane.

$$\Delta w = \frac{\partial^2 w}{\partial x^2} + \frac{\partial^2 w}{\partial y^2} = \frac{a}{A_0}\frac{(uw)}{x(x^2+y^2)}\left(5 + 2\left(\frac{x^2+y^2}{xy}\right)^2\right) = \frac{a}{A_0}\frac{(vw)}{y(x^2+y^2)}\left(5 + 2\left(\frac{x^2+y^2}{xy}\right)^2\right). \quad (45)$$

We used (25) in (45).

The main theorem of tunnel mathematics allows to find the temperature distribution for planes $z = const$ (it is similar to the constructing of slices of brain at MRI procedure). Further, collecting these "slices", we can obtain full spatial distribution of the temperature around a supersonic cone.

4.2.1.1 Equation of continuity

For compressible fluid the density ρ is the variable quantity, which is to be determined from equation of continuity:

$$\rho \boldsymbol{div}\vec{V} + \vec{V}\boldsymbol{grad}\rho = 0. \quad (46)$$

Taking into account (16), (32) – (34) we can obtain such relation for the divergence of velocity field:

$$\nabla \cdot \vec{V} = \boldsymbol{div}\vec{V} = \frac{\partial u}{\partial x} + \frac{\partial v}{\partial y} + \frac{\partial w}{\partial z} = 2\left(\frac{A_0}{a} + \frac{A_1}{R\cos\theta}(v_R \sin\theta + v_\theta \cos\theta)\right). \quad (47)$$

We will seek the solution of our problem on the plane

$$z = R\sin\theta = const = 0.5. \quad (48)$$

Direction of motion is shown below in Figure 19.

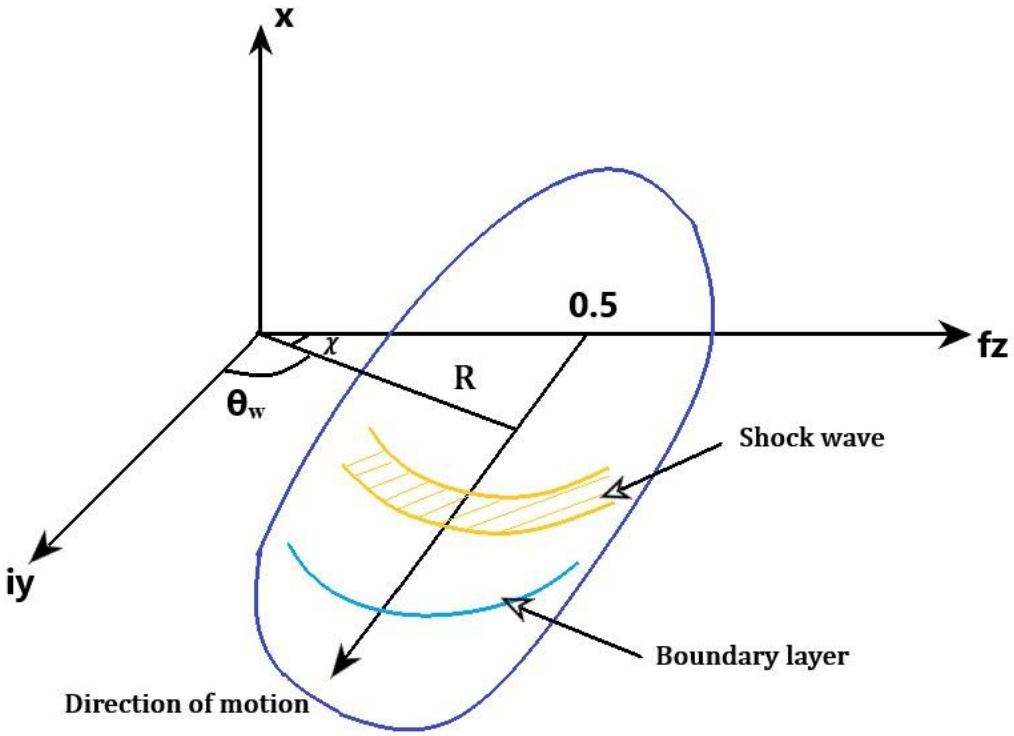

Figure 19. Direction of motion on the plane $z = 0.5$ (χ is a half of vertical angle of cone; $\theta_w = \frac{\pi}{2} - \chi$ is the angle θ corresponding to the wall of cone).

Analyzing (40) and (41) we see that it is easier to fulfill the integration of (46) by dR than by $d\theta$. So, taking differential from (48) we obtain such relation:

$$d\theta = -\frac{\tan\theta}{R}dR. \quad (49)$$

Further, we integrate (46) in front of the shock wave (i. e. applying formulas (37) for incident flow) and behind the shock wave (i. e. applying formulas (40) and (41) for reflected flow).
Finally, we obtain such relations. In front of the shock wave:

$$\rho = \rho_0 \left(\frac{R}{R_0}\right)^{\frac{2A_1 \tan\theta}{\cos 2\theta}} \cdot \exp\left[0.5 \cdot \frac{2A_0}{a v_0 \cos 2\theta}\right]; \tag{50}$$

where R_0 is a constant, $[R_0] = m$; ρ_0 is a density of fluid at $R \to \infty, \theta \to 0, [\rho_0] = \frac{kg}{m^3}$.
Behind the shock wave:

$$\rho = \rho_0 \left(\frac{R}{R_0}\right)^{\frac{2A_1 \delta \tan\theta}{\gamma}} \cdot \exp\left[0.5 \cdot \frac{2A_0}{5(1-\alpha)\beta\gamma\xi R_1 A_0} \cdot R^{4-5\alpha}\right]$$
$$= \rho_0 \left(\frac{R}{R_0}\right)^{\frac{2A_1 \delta \tan\theta}{\gamma}} \cdot \exp\left[0.5 \cdot \frac{2A_0}{5(1-\alpha)R_1} (v_\theta - v_R \tan\theta)^{-1}\right]; \tag{51}$$

where R_1 is a constants, $[R_1] = m$; $v_R \; and \; v_\theta$ are taken from (40) and (41); besides,

$$\alpha = \frac{tan\,\theta}{tan\,\theta_w}; \tag{52}$$
$$\beta = \frac{2}{A_2(\cos\theta)^4}\left[\frac{A_2(\cos\theta_w)^5}{2}\right]^{\alpha}; \tag{53}$$
$$\gamma/\delta = \cos\theta\,(tan\,\theta_w)^{\alpha} \;\; -/+ \;\; \sin\theta\tan\theta\;\; (tan\,\theta_w)^{-\alpha} \cdot \cos\pi\alpha\,; \tag{54}$$
$$\xi = \frac{(r_0 a)^2}{((r_0 a)^2 a)^{\alpha}}; [\xi] = m^{4-5\alpha}. \tag{55}$$

The graphs corresponding to (50) and (51) are shown below in Figure 20.

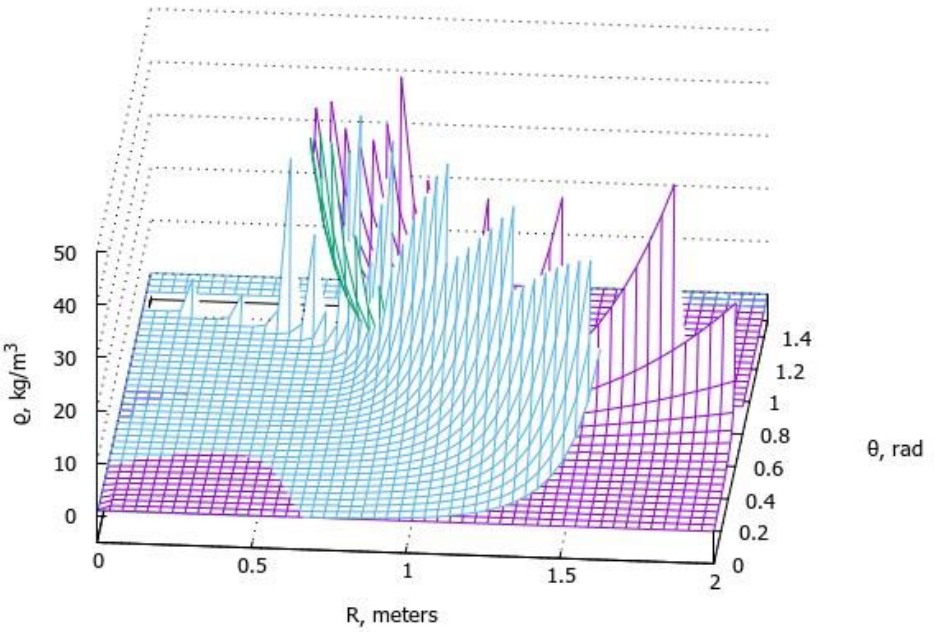

Figure 20. The graphs corresponding to (50) (blue) and (51) (cyan) at $\chi = 10°$ ($\theta_w = 80°$ ($1.4\,rad$)) and $v_0 = 500\ \frac{m}{sec}$ (supersonic case).

Constructing graphs in Figs. 20 we assume for constants in (50) and (51) such values:

$\rho_0 = 1\ \frac{kg}{m^3}$; (density of air at $T \approx 300\ K, p \approx 10^5 Pa$);
$R_0 = 1\ m$;
$R_1 = 1\ m$;
$A_1 = 1$;
$A_0 = v_0 = 500\ \frac{m}{sec}$;
$r_0 = 1\ m$;
$a = 10\ m$;
$\theta_w = 80°\ (1.4\ rad)$.

Comparing Figs. 20 and 19, we see that at $R \approx 0.5\ m$ and $\theta \approx \theta_w = 1.4\ rad$ density reaches several peaks. This behavior of density can be explained by compressibility of fluid past a cone. Further in a certain range of coordinates R and θ, the shock wave extends. It is obviously that shock wave has a certain thickness. The Figure 21 below shows a graph corresponding to (51) separately, where the cascading air density is clearly tracked on the plane $z = 0.5$ of supersonic cone.

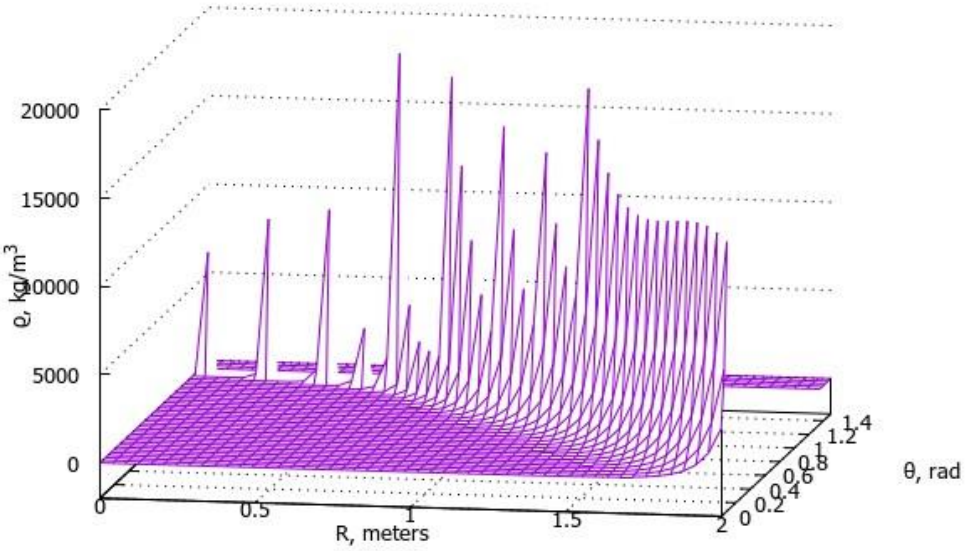

Figure 21. The graph corresponding to (51) at $\chi = 10°$ ($\theta_w = 80°\ (1.4\ rad)$) and $v_0 = 500\ \frac{m}{sec}$ (supersonic case).

4.2.1.2 Navier-Stokes equations for a compressible flow.

For a supersonic compressible flow, the dynamic viscosity μ must be regarded as dependent on the space coordinate, because μ varies considerably with temperature, and the changes in velocity and pressure together with the heat due to friction bring about considerable temperature variations.

So, in Cartesian coordinate system the Navier-Stokes equations for a compressible flow look like this ([2], we neglect by gravitational forces comparing with pressure and thermal forces):

$$\rho\frac{Du}{Dt}=-\frac{\partial P}{\partial x}+\frac{\partial}{\partial x}\left(\mu\left(2\frac{\partial u}{\partial x}-\frac{2}{3}\boldsymbol{div}\vec{V}\right)\right)+\frac{\partial}{\partial y}\left(\mu\left(\frac{\partial u}{\partial y}+\frac{\partial v}{\partial x}\right)\right)+\frac{\partial}{\partial z}\left(\mu\left(\frac{\partial w}{\partial x}+\frac{\partial u}{\partial z}\right)\right);\ (56)$$

$$\rho\frac{Dv}{Dt}=-\frac{\partial P}{\partial y}+\frac{\partial}{\partial y}\left(\mu\left(2\frac{\partial v}{\partial y}-\frac{2}{3}\boldsymbol{div}\vec{V}\right)\right)+\frac{\partial}{\partial z}\left(\mu\left(\frac{\partial v}{\partial z}+\frac{\partial w}{\partial y}\right)\right)+\frac{\partial}{\partial x}\left(\mu\left(\frac{\partial u}{\partial y}+\frac{\partial v}{\partial x}\right)\right);\ (57)$$

$$\rho\frac{Dw}{Dt}=-\frac{\partial P}{\partial z}+\frac{\partial}{\partial z}\left(\mu\left(2\frac{\partial w}{\partial z}-\frac{2}{3}\boldsymbol{div}\vec{V}\right)\right)+\frac{\partial}{\partial x}\left(\mu\left(\frac{\partial w}{\partial x}+\frac{\partial u}{\partial z}\right)\right)+\frac{\partial}{\partial y}\left(\mu\left(\frac{\partial v}{\partial z}+\frac{\partial w}{\partial y}\right)\right).\ (58)$$

The equation for temperature variations has such form ([2]):

$$\rho c_p\frac{dT}{dt}=\frac{dP}{dt}+\frac{\partial}{\partial x}\left(k\frac{\partial T}{\partial x}\right)+\frac{\partial}{\partial y}\left(k\frac{\partial T}{\partial y}\right)+\frac{\partial}{\partial z}\left(k\frac{\partial T}{\partial z}\right)+\mu\Phi;\qquad(59)$$

where $\frac{D}{Dt}$, $\frac{d}{dt}$ are the substantial derivatives; T is a temperature; $c_p\ [J/kg\ K]$ represents the specific heat at constant pressure per unit mass (in general c_p depends on temperature, but we will assume its value as a constant equal to *1090* $J/kg\ K$ (the air at *800 K*)); $k\ [J/m\ sec\ K]$ is a thermal conductivity; $\Phi\ [1/sec^2]$ represents the dissipation function:

$$\Phi=2\left(\left(\frac{\partial u}{\partial x}\right)^2+\left(\frac{\partial v}{\partial y}\right)^2+\left(\frac{\partial w}{\partial z}\right)^2\right)+\left(\frac{\partial u}{\partial y}+\frac{\partial v}{\partial x}\right)^2+\left(\frac{\partial v}{\partial z}+\frac{\partial w}{\partial y}\right)^2+\left(\frac{\partial w}{\partial x}+\frac{\partial u}{\partial z}\right)^2-\frac{2}{3}\left(\frac{\partial u}{\partial x}+\frac{\partial v}{\partial y}+\frac{\partial w}{\partial z}\right)^2.\qquad(60)$$

We assume that both the viscosity μ and the thermal conductivity k for supersonic case depend from the temperature in such manner:

$$\mu=\mu_0\left(\frac{T}{T_0}\right)^n;\qquad(61)$$

$$k=k_0\left(\frac{T}{T_0}\right)^n;\qquad(62)$$

where $\mu_0=0.00001\ Pa\cdot sec$; $k_0=0.0242\ \frac{J}{m\sec K}$; $T_0=300\ K$ (temperature of incident flow); n is a real number. We introduced (62) in order to eliminate from our considerations the Prandtl's number.

The equations (56) – (58) acquires such tensor form for steady motion of fluid:

$$\rho v_k\frac{\partial v_i}{\partial x_k}=-\frac{\partial P}{\partial x_i}+\mu\left(\frac{\partial^2 v_i}{\partial x_k\partial x_k}+\frac{1}{3}\frac{\partial}{\partial x_i}\left(\frac{\partial v_l}{\partial x_l}\right)\right)+\left(\frac{\partial v_i}{\partial x_k}+\frac{\partial v_k}{\partial x_i}-\frac{2}{3}\delta_{ik}\frac{\partial v_l}{\partial x_l}\right)\times\left(\frac{\partial\mu}{\partial x_k}\right);\ (63)$$

where δ_{ik} is the Kronecker symbol: $\delta_{ik}=\begin{cases}1, if\ i=k;\\0, if\ i\neq k.\end{cases}$
Last term in (63) represent a tensor product.

So, Navier-Stokes equations (56) – (59) in modified (1) spherical polar coordinates assume such form:

$$\begin{aligned}&\rho\left(v_R\frac{\partial v_R}{\partial R}+v_\theta\frac{\partial v_R}{R\partial\theta}-\frac{v_\theta^2}{R}\right)\\&=-\frac{\partial P}{\partial R}+\mu\left(\Delta v_R-\frac{2v_R}{R^2}-\frac{2}{R^2\cos\theta}\frac{\partial(v_\theta\cos\theta)}{\partial\theta}+\frac{1}{3}\frac{\partial}{\partial R}\left(\boldsymbol{div}\vec{V}\right)\right)\\&\qquad+2\frac{\partial\mu}{\partial R}\left(\frac{\partial v_R}{\partial R}-\frac{1}{3}\boldsymbol{div}\vec{V}\right)-\frac{\partial\mu}{R\partial\theta}\left(\frac{\partial v_R}{R\partial\theta}+\frac{\partial v_\theta}{\partial R}-\frac{v_\theta}{R}\right);\end{aligned}\qquad(64)$$

$$\begin{aligned}&\rho\left(v_R\frac{\partial v_\theta}{\partial R}+v_\theta\frac{\partial v_\theta}{R\partial\theta}+\frac{v_Rv_\theta}{R}\right)\\&=\frac{\partial P}{R\partial\theta}-\mu\left(\Delta v_\theta-\frac{2}{R^2}\frac{\partial v_R}{\partial\theta}+\frac{v_\theta}{(R\cos\theta)^2}+\frac{1}{3}\frac{\partial}{R\partial\theta}\left(\boldsymbol{div}\vec{V}\right)\right)\\&\qquad+\frac{\partial\mu}{\partial R}\left(\frac{\partial v_R}{R\partial\theta}+\frac{\partial v_\theta}{\partial R}-\frac{v_\theta}{R}\right)-2\frac{\partial\mu}{R\partial\theta}\left(\frac{\partial v_\theta}{R\partial\theta}+\frac{v_R}{R}-\frac{1}{3}\boldsymbol{div}\vec{V}\right);\end{aligned}\ (65)$$

$$\rho c_p\left(v_R\frac{\partial T}{\partial R}+v_\theta\frac{\partial T}{R\partial\theta}\right)=v_R\frac{\partial P}{\partial R}+v_\theta\frac{\partial P}{R\partial\theta}+k_0\left(\frac{T}{T_0}\right)^n\left(\frac{1}{R^2}\frac{\partial}{\partial R}\left(R^2\frac{\partial T}{\partial R}\right)+\frac{1}{R^2\cos\theta}\frac{\partial}{\partial\theta}\left(\cos\theta\frac{\partial T}{\partial\theta}\right)\right)+$$
$$\frac{k_0 n}{T_0}\left(\frac{T}{T_0}\right)^{n-1}\left(\left(\frac{\partial T}{\partial R}\right)^2+\left(\frac{\partial T}{R\partial\theta}\right)^2\right)+\mu_0\left(\frac{T}{T_0}\right)^n\Phi. \quad (66)$$

The equation with v_φ disappears. Laplacians Δv_R and Δv_θ in (64) and (65) are the spatial ones.

Using (60), (32) – (34) and (45) we arrive to the following relation for the dissipation function in (66):

$$\Phi=2\left(2\left(\frac{A_0}{a}\right)^2+\left(\boldsymbol{div}\vec{V}-\frac{2A_0}{a}\right)^2\right)+\frac{(uw)}{x}\left(\Delta w-\frac{(uw)(x^2+y^2)}{x(xy)^2}\right)-\frac{2}{3}\left(\boldsymbol{div}\vec{V}\right)^2. \quad (67)$$

Relation (67) works on the plane $z=const$.

4.2.2 Calculation of the temperature distribution.
As we have already found the components of vector velocity field v_R and v_θ, we need, in principle, only the equations (64) and (65) to find the temperature distribution around supersonic cone. Equation (66) can be used for auxiliary goals. The main theorem of tunnel mathematics, which is expressed in the equation (4), allows to integrate equations (64) and (65) on our plane $z=0.5$. In order to do this, we vary in (64) and (65) the variable of integration $d\theta$ by dR using (49), after what we eliminate pressure P from these equations. Finally, we arrive to the following simple ordinary differential equation for dynamic viscosity (and consequently for the temperature (61)) in the area behind the shock wave:

$$\alpha_1\frac{\partial\mu}{\partial R}+\gamma_1\mu-\beta_1=0; \quad \textbf{(68)}$$

where

$$\alpha_1=\frac{\partial v_R}{\partial R}(3-(\tan\theta)^{-2})+(\tan\theta)^{-1}\frac{\partial v_\theta}{\partial R}(3-(\tan\theta)^2)-\frac{2v_R}{R}$$
$$+(\tan\theta)^{-1}\frac{v_\theta}{R}((\tan\theta)^2-1); \quad \textbf{(69)}$$

$$\gamma_1=\Delta v_R+(\tan\theta)\Delta v_\theta+\frac{2}{R\tan\theta}\left(\frac{\partial v_\theta}{\partial R}+\tan\theta\frac{\partial v_R}{\partial R}\right)-\frac{2v_R}{R^2}+\frac{v_\theta\tan\theta}{(R\cos\theta)^2}; \quad (70)$$

$$\beta_1=\rho\left(\left(\frac{\partial v_R}{\partial R}-\tan\theta\frac{\partial v_\theta}{\partial R}\right)(v_R-v_\theta(\tan\theta)^{-1})-\frac{v_\theta\tan\theta}{R}(v_R+v_\theta(\tan\theta)^{-1})\right). \quad (71)$$

Laplacians Δv_R *and* Δv_θ in (70) now should be calculated on the plane $z=const$, not in the space.

Similar to the case of a compressible fluid entrained by hypersonic rotating disk in [15] we have again got very simple differential equation for the temperature distribution.

Someone can notice that we had not the right to integrate equations (64) and (65) on the plane $z=const$ in such simple way. To which we dare to object that spatial expressions (40) and (41) for v_R and v_θ in the area behind the shock wave *are not spatial in the full sense of the word*. They have been obtained by means relations of tunnel mathematics (2) – (4) which *in specific way take into account the variations of* v_R *and* v_θ *on the plane*
$z=const$. So, fulfilling the integration of Navier-Stokes equations on the plane, we can consider variables R and θ *as independent*, what allows to simplify the integration significantly!

In order to simplify our calculations, we will seek such analytical solution of (68) which is more accurate in the vicinity of

$$\alpha = \frac{\tan\theta}{\tan\theta_w} = \frac{2}{3} \approx 0.6. \tag{72}$$

To find, for instance, exact analytical solution of (68) in the vicinity of cone wall additional terms must be taken into account.

Using relations (18), (20) – (22), (23), (24), (32), (33), (34), (40), (41), (45) and (61) we arrive to the following approximate analytical solution of (68):

$$T = T_o\left(\frac{1}{\mu_0}R_2^{\delta_6}R^{-(2+\delta_6)}\cdot(\alpha_6(\rho-\beta_6R^{-2}\rho')+R^2C)\cdot\exp\left[\frac{0.5\sin\theta}{5(\alpha-1)}\Sigma\right]\right)^{\frac{1}{n}}; \tag{73}$$

where the density ρ is taken from (51); besides,

$$\rho' = \rho_0\exp[0.5\delta_4'R]\,;\ \rho' \text{ is the } \textit{oscillating density}; \tag{74}$$

$$C = \mu_0\left(\frac{T_w}{T_0}\right)^n\ ; \text{ where } T_w \text{ is the temperature of the cone wall; } T_0 \text{ is the temperature of incident flow;} \tag{75}$$

$$\Sigma = \left(R\left(\frac{\partial v_R}{\partial R}(3-(\tan\theta)^{-2})+\frac{\partial v_\theta}{\partial R}\cot\theta\,(3-(\tan\theta)^2)\right)+v_\theta\cot\theta\,((\tan\theta)^2-1)-2v_R\right)^{-1}\times\left(\frac{A_0}{a}(2-(\cos\theta)^{-2})-\frac{4A_3a}{A_0(\cos\theta)^3}\left((v_R^2-v_\theta^2)\frac{\sin 2\theta}{2}+v_Rv_\theta\cos 2\theta\right)\cdot R^{-2}\right); \tag{76}$$

In (76) Σ is the *vortical factor*; $v_R, v_\theta, \frac{\partial v_R}{\partial R}, \frac{\partial v_\theta}{\partial R}$ are taken from (40) and (41).

$$R_2 \approx \begin{cases}0.51\ for\ \theta_w = 80°\ (1.4\ rad);\\ 0.53\ for\ \theta_w = 70°\ (1.2\ rad);\end{cases} \tag{77}$$

$$\alpha_6 = \frac{\beta_4}{\gamma_3\delta_4};\ \beta_6 = (R_0^{\gamma_4}\delta_4)^{-1}; \tag{78}$$

$$\gamma_4 = 10(1-\alpha); \tag{79}$$

$$\beta_4 = (A_0\gamma_2\delta_2\sin\theta)^2\alpha_4;\ [\beta_4] = \left(\frac{m}{sec}\cdot m^{4-5\alpha}\right)^2; \tag{80}$$

$$\alpha_4 = ((\tan\theta_w)^{-\alpha}\cos\pi\alpha-(\tan\theta_w)^\alpha)\cdot((\tan\theta_w)^{-\alpha}\cos\pi\alpha-(\cot\theta)^2(\tan\theta_w)^\alpha)-(\tan\theta_w)^\alpha\cdot((\tan\theta_w)^{-\alpha}\cos\pi\alpha+(\cot\theta)^2(\tan\theta_w)^\alpha); \tag{81}$$

$$\gamma_3 = A_0\gamma_2\delta_2\big((5\alpha-4)\alpha_3+\beta_3\big);\ [\gamma_3] = \frac{m}{sec}\cdot m^{4-5\alpha}; \tag{82}$$

$$\alpha_3 = \sin\theta\,(\tan\theta_w)^{-\alpha}(\cos\pi\alpha)\,(3-(\tan\theta)^{-2})+\frac{(\cos\theta)^2}{\sin\theta}(\tan\theta_w)^\alpha(3-(\tan\theta)^2); \tag{83}$$

$$\beta_3 = \frac{(\cos\theta)^2}{\sin\theta}(\tan\theta_w)^\alpha((\tan\theta)^2-1)-2\sin\theta\,(\tan\theta_w)^{-\alpha}\cos\pi\alpha\,; \tag{84}$$

$$\delta_4 \approx \delta_4' = \frac{2A_0}{5(1-\alpha)\beta\gamma\xi R_1A_0};\ [\delta_4] = [\delta_4'] = (m\cdot m^{4-5\alpha})^{-1} \approx m^{-2}; \tag{85}$$

$$A_0 = v_0 = 500\ \frac{m}{sec}; \tag{86}$$

$$a = 100\ m; \tag{87}$$

$$A_3 = \frac{4}{A_2^2}-\frac{1}{A_2}+2; \tag{88}$$

$$\gamma_2 = \frac{2(r_0a)^2}{A_2(\cos\theta)^4};\ [\gamma_2] = m^4; \tag{89}$$

$$\delta_2 = \left[\frac{A_2(\cos\theta_w)^5}{2(r_0a)^2a}\right]^\alpha;\ [\delta_2] = m^{-5\alpha}; \tag{90}$$

$$\delta_6 = \frac{A_0\gamma_2\delta_2\lambda_2}{\gamma_3}; \tag{91}$$

$$\lambda_2 = 2(5\alpha - 4)\xi_2 + \sin\theta\,\zeta_2; \quad (92)$$

$$\xi_2 = \sin\theta\,(tan\,\theta_w)^{-\alpha}\cos\pi\alpha + \frac{\cos\theta}{\tan\theta}(tan\,\theta_w)^{\alpha}; \quad (93)$$

$$\zeta_2 = \frac{(tan\,\theta_w)^{\alpha}}{(\cos\theta)^2} - 2(tan\,\theta_w)^{-\alpha}\cos\pi\alpha\,; \quad (94)$$

The constant C were selected in such a way as to satisfy the following boundary conditions for (73) on the plane $z = 0.5$:

$$T = T_w \text{ at } \begin{cases} R \approx 0.51\ for\ \theta = \theta_w = 80°\ (1.4\ rad); \\ R \approx 0.53\ for\ \theta = \theta_w = 70°\ (1.2\ rad); \end{cases} \quad (95)$$

Below in Figs. 22 and 23 the graphs corresponding to (73) are shown for $\chi = 10°$ ($\theta_w = 80°\ (1.4\ rad)$) and $\chi = 20°$ ($\theta_w = 70°\ (1.2\ rad)$) respectively at $v_0 = 500\ \frac{m}{sec}$ (supersonic case).

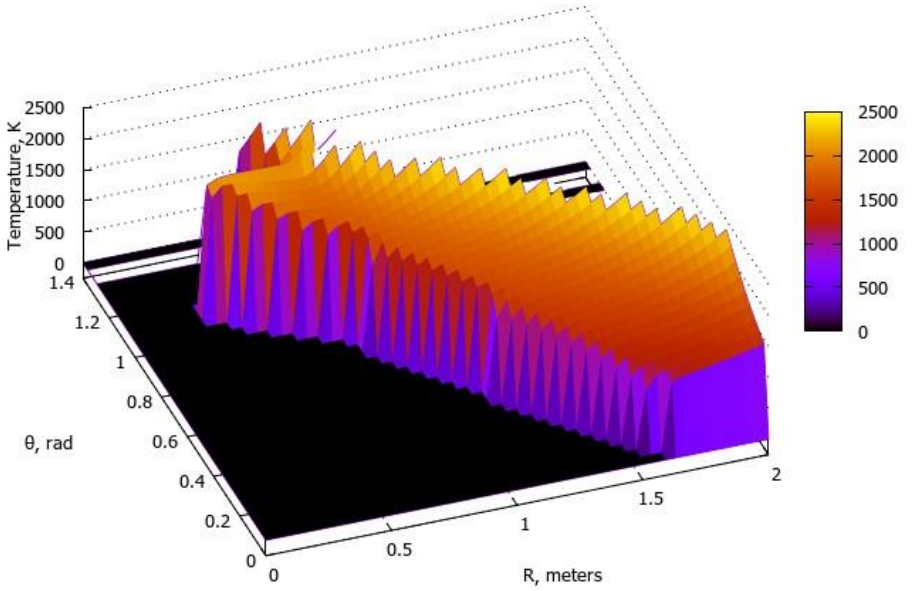

Figure 22. The graph corresponding to (73) at $\chi = 10°$ ($\theta_w = 80°\ (1.4\ rad)$) and $v_0 = 500\ \frac{m}{sec}$ (supersonic case).

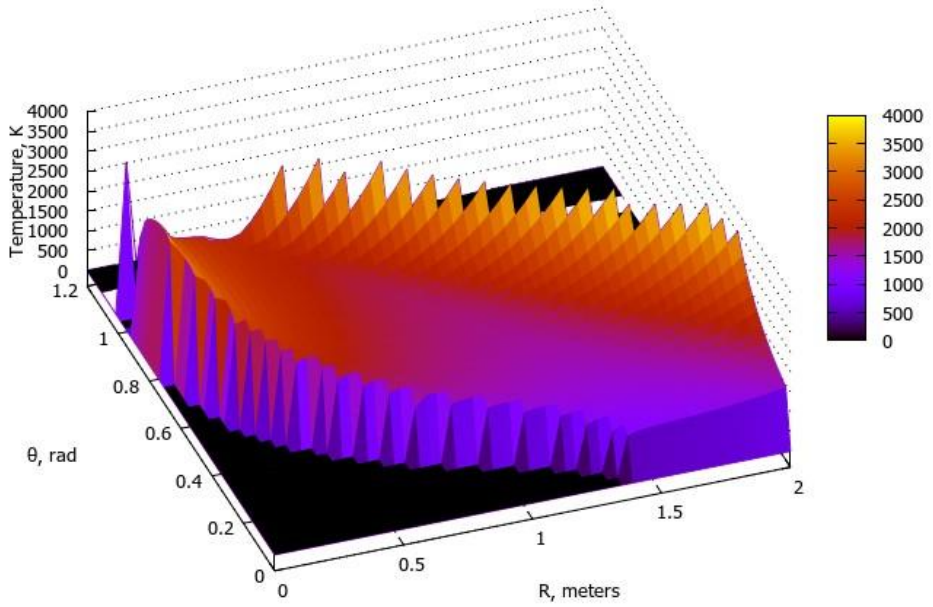

Figure 23. The graph corresponding to (73) at $\chi = 20°$ ($\theta_w = 70°\ (1.2\ rad)$) and $v_0 = 500\ \frac{m}{sec}$ (supersonic case). (This graph should be shifted by approximately 0.53 m along *R* axis.)

When constructing the graphs in Figs. 22 and 23 we assume for constants in (73) such values:
$T_0 = 300\ K;$
$T_w = \begin{cases} 1000\ K\ for\ \theta_w = 80°\ (1.4\ rad); \\ 1200\ K\ for\ \theta_w = 70°\ (1.2\ rad); \end{cases}$
$\mu_0 = 0.00001\ Pa \cdot sec;$
$\rho_0 = 1\ \frac{kg}{m^3}$; (density of air at $T \approx 300\ K, p \approx 10^5 Pa$);
$R_0 = 1\ m;\ R_1 = 1\ m;$
$A_1 = 2;\ A_2 = 1;\ A_3 = 5;$
$A_0 = v_0 = 500\ \frac{m}{sec};$
$r_0 = 1\ m;$
$a = 100\ m;$
R_2 is taken from (77);
$n = 21.$

When constructing the graphs in Figs. 22 and 23 we used for last factor in (73) the approximate relation $e^x \approx 1 + x$. Graphs are somewhat blurred due to the simplifications we have adopted.

It is easy seen from Figs. 22 and 23 that for a supersonic cone the temperature distribution in the plane $z = 0.5$ is cascading and reaches a maximum on the cone wall. This differs from the case of hypersonic rotating disk where the temperature of air reaches a maximum on some distance from the surface of disk [15]. Besides, the temperature profiles in Figs. 22 and 23 have different curvature. Rather large value of the exponent in (61) ($n = 21$) can probably be explained by the choice of calibration coefficients $a, A_1, A_2, A_3, r_0, R_0\ and\ R_1$.

Substituting in (73) corresponding value of *z* we can obtain full spatial distribution of the temperature around a supersonic cone. After what it will be possible to carry out the comparison of this distribution with experimental data. For instance, it is well-known at this moment that heat generation within the hypersonic boundary layer occurs due to dilatation and shear processes [13]. Dilatation heating, due to pressure, dominates the early transitional high-temperature region. Shear-induced heating is the dominant process creating the latter high-temperature region, where the transition is almost complete. Zhu et al. [13] showed that the dilatation heating in the first high-temperature region of a smooth flared cone is more than five times its shear counterpart. We think that tunnel mathematics has ample means to model this result. So, new field for further investigations opens.

4. Conclusion

The solution of the Navier-Stokes equations using the tunnel mathematics apparatus is both simple and elegant, requiring strong mathematical training and a deep physical analysis of the problem. This method does not require special software and can be applied for the primary analysis of hydrodynamic problems. The results obtained for a supersonic cone make it possible to qualitatively estimate the thickness of the boundary layer, the shape of the shock wave, and whether the shock wave intersects the boundary layer. It was found that the lower the velocity of the incident flow and the larger the vertex angle of the cone, the smaller the values of the angles θ the shock wave acquires. Additionally, the smaller the vertex angle of the cone and the higher the velocity of the incident flow, the more the shape of the shock wave resembles a right cone. This behavior of the shock wave fully corresponds to the physical pattern of the phenomena. Furthermore, we obtained a simple expression for the temperature distribution on the plane z = const. By compiling these plane distributions, we can obtain the full spatial distribution of temperature around a supersonic cone. In this expression, we introduced two new definitions: oscillating density ρ^' and vortical factor Σ. This expression for the temperature distribution was derived by considering all terms in the original Navier-Stokes equations for compressible flow, without exceptions. Therefore, this expression holds certain methodological interest.

5. References

[1] Hantsche, W., & Wendt, H. (1942). Cones in supersonic flow (Mit Uberschallgeschwindigkeit angeblasene Kegelspitzen). Jahrbuch der deutschen Luftfahrtforschung, 180–190.

[2] Jiaming Yu, Y., Zhu, Y., Gu, D., & Lee, C. (2022). A thermoacoustic heat pump driven by acoustic waves in a hypersonic boundary layer. *Physics of Fluids, 34*(1), 011703. **https://doi.org/10.1063/5.0079611**

[3] Kochin, N. E., Kibel, I. A., & Roze, N. V. (1964). *Theoretical Hydromechanics* (Part 2, § 27). John Wiley & Sons Ltd.

[4] Landau, L. D., & Lifshitz, E. M. (1987). *Fluid Mechanics* (2nd ed.). Pergamon Press.

[5] Lavrentiev, M., & Chabat, B. (1972). *Méthodes de la théorie des fonctions d'une variable complexe* (Transl. from Russian). Mir.

[6] Lee, C., & Chen, S. (2018). Recent progress in the study of transition in the hypersonic boundary layer. *National Science Review, 6*, 155.

[7] Maccoll, J. W., & Taylor, G. I. (1933). The air pressure over a cone moving at high speeds. *Proceedings of the Royal Society, 139*, 278-311. **https://doi.org/10.1098/rspa.1933.0017**

[8] Maccoll, J. W. (1937). The conical shock wave formed by a cone moving at a high speed. *Proceedings of The Royal Society A: Mathematical, Physical and Engineering Sciences, 159*, 459-472.

[9] Schlichting, H. (1979). *Boundary-Layer Theory* (7th ed.). McGraw Hill.

[10] Shvydkyi, O. G. (2022a). Analytical solution of the steady Navier-Stokes equation for an incompressible fluid entrained by a rotating disk of finite radius using the apparatus of tunnel mathematics. **https://doi.org/10.21203/rs.3.rs-1346916/v2**

[11] Shvydkyi, O. G. (2022b). Analytical solution to the steady Navier-Stokes equation for a compressible fluid entrained by a rotating disk of finite radius in the area of boundary layer by means of tunnel mathematics (subsonic and hypersonic cases). **https://doi.org/10.21203/rs.3.rs-2310304/v1**

[12] Shvydkyi, O. G. (2022c). Tensor foundations of tunnel mathematics. **https://doi.org/10.21203/rs.3.rs-2827573/v1**

[13] Smith, C. R. C. (2021). Aerodynamic heating in hypersonic flow. *Physics Today, 74*(11), 66. **https://doi.org/10.1063/PT.3.4888**

[14] Unnikrishnan, S., & Gaitonde, D. (2016). Acoustic, hydrodynamic, and thermal modes in a supersonic cold jet. *Journal of Fluid Mechanics, 800*, 387-432. **https://doi.org/10.1017/jfm.2016.410**

[15] von Kármán, T., & Moore, N. B. (1932). Resistance of slender bodies moving with supersonic velocities, with special reference to projectiles. *ASME Transactions, 54*, 303.

[16] Zhu, Y., Lee, C., Chen, X., Wu, J., Chen, S., & Gad-el-Hak, M. (2018). Newly identified principle for aerodynamic heating in hypersonic flows. *Journal of Fluid Mechanics, 855*, 152-180. **https://doi.org/10.1017/jfm.2018.646**

6. Conflict of Interest

The author declare no competing conflict of interest.

7. Funding

No funding was received to support this study.

8. Author Information

Oleh G. Shvydkyi graduated from Zaporizhia State University with a degree in Solid State Physics, specializing in magnetism. He spent five years working as a process engineer in the laboratory of metal physics at the Motor-Sich Aviation Plant in Zaporizhia, Ukraine. There, he conducted research on heat-resistant steels using electron microscopy. Currently, Shvydkyi works as an independent researcher, developing a new mathematical approach called tunnel mathematics, which is based on the theory of complex variables, to find physically admissible solutions to the Navier-Stokes equations.